Pulsatile shear and Gja5 modulate arterial identity and remodeling events during flow-driven arteriogenesis

Supplementary Material

Fig. S1. Hemodynamic signals in chicken embryo yolk sac arteries and veins at the 30-somite stage. (**A**) Time-averaged mean red blood cell velocity increases with diameter in yolk sac arteries and veins. (**B**) Mean shear rates are relatively constant for both arteries and veins. Regression line (solid lines) and 95% confidence interval (dotted lines) are indicated; regression coefficients are not significant. (**C**) Maximal red blood cell acceleration rate in arteries and veins. (**D**) Maximal acceleration rate as a function of mean velocity separates arterial from venous vessels.

Fig. S2. Receiver operator characteristics (ROC) analysis. Results of a receiver operator characteristics (ROC) analysis of the relative pulse slope index (RPSI) for the discrimination of arteries from veins. The top panel gives the ROC curve with an ROC area under the curve (AUC) of 0.98 (s.e.=0.011, $P<0.0001$). An AUC of 1 indicates a perfect separation, whereas a random selection (corresponding to the diagonal dashed line in the graph) exhibits an AUC value of 0.5. The middle panel shows the dependence of accuracy of discrimination of arteries from veins from the chosen critical RPSI value. The accuracy of discrimination is calculated by the Youden Index (J=maxSEi + SPi−1, where SEi and SPi are the sensitivity and specificity for a given RPSI value). The maximum accuracy value of J=0.8928 is achieved for an RPSI of 7.909 and is marked by a circle in both panels. The discrimination of arteries and veins by this RPSI value (gray horizontal line, 7.9) is shown on the dot diagram in the bottom panel. RPSI is given in seconds^{-1}.

Fig. S3. Hemodynamic signals in chicken embryo yolk sac arteries and veins at the 22- and 44-somite stages. (**A-C**) Time-averaged mean red blood cell velocity (A), mean shear rates (C) and maximal red blood cell acceleration rates (B) in yolk sac arteries and veins in 22- and 44-somite stage chicken embryos. (**D**,**E**) Maximal acceleration rate as a function of mean velocity (E), and RPSI (D) separate arterial from venous vessels. (**F**) RPSI was significantly higher in arteries than veins at both the 22- and 44-somite stage. ***, $P<0.001$;,Mann Whitney U-test.

Fig. S4. Role of oxygen in yolk sac remodeling. (**A**) In vivo measurements of oxygen saturation show significantly lower levels in arteries than veins. (**B**) Exposing developing embryos to an ambient oxygen level of 10% O_2 (hypoxia) impairs yolk sac arterial network growth (red arrow) as compared with exposure to 21% O_2 (normoxia). LVA, left vitelline artery; RVA, right vitelline artery.

Fig. S5. Role of oxygen in yolk sac remodeling. (**A**) In vivo measurements of oxygen saturation show significantly lower levels in arteries than veins. (**B**) Exposing developing embryos to an ambient oxygen level of 10% O_2 (hypoxia) impairs yolk sac arterial

network growth (red arrow) as compared with exposure to 21% O_2 (normoxia). LVA, left vitelline artery; RVA, right vitelline artery.

Fig. S6. Gja5 (connexin 40) expression in mouse arteries. Imaging arterial expression of Gja5 (connexin 40) in yolk sac, hindlimb and brain using connexin 40-EGFP knockin reporter mice. ACA, anterior cerebral artery; MCA, middle cerebral artery; PComA, posterior communicating artery.

Fig. S7. MicroCT imaging of collateral arterial networks after femoral artery occlusion. (**A**,**B**) Schematic overview of the regions of interest in the occluded right hindlimb (A) and control left hindlimb (B). (A) Femoral artery occlusion will result in shunting of blood flow through pre-existing collateral arteries. Increased blood flow causes outward remodeling leading to a diameter increase. The growing arterial collaterals (blue arrows) were detected between the deep femoral artery and the lateral caudal femoral artery (region of interest 1), and between the lateral caudal femoral artery and saphenous artery (region of interest 2). (B) Pre-existing collateral arteries in the control hindlimb (green arrows) were analyzed at anatomically comparable positions. (**C-F**) Representative microCT scans showing the arterial network in the occluded right hindlimb in wild-type (C,D) and *Gja5*$^{-/-}$ (E,F) mice. (C,E) Overview images showing the position of the major arteries (red arrowheads with legends) and arterial collaterals (blue arrows) in the occluded right hindlimb of wild-type and *Gja5*$^{-/-}$ mice. (D,F) Focus on the growing collaterals (blue arrows) in the occluded right hindlimb in wild-type and *Gja5*$^{-/-}$. (**G**) Collateral arterial diameters were significantly smaller in *Gja5*$^{-/-}$ than wild type. (**H**) Diameters of pre-existing collateral arteries did not differ between *Gja5*$^{-/-}$ and wild type. ROI, region of interest. *, $P<0.05$, Student's *t*-test.

Fig. S8. Reduced flow-induced outward remodeling in *Gja5*$^{b>-/b>/b>-}$ arteries. (**A**) Schematic overview of the mesenteric ligation model. Ligation of second-order mesenteric resistance arteries (arrows) creates two low-flow (LF) arteries. As a consequence of these ligations, blood flow is shunted to a third artery, which is now exposed to high flow (HF artery). Normal flow (NF) arteries derived from a position remote from the ligation site were used as control. Subsequently, arterial segments were mounted in a pressure mygraph and passive pressure-diameter curves established under maximal vasodilatory conditions. (**B**) After 7 days exposure to high blood flow (HF arteries), arteries from *Gja5*$^{-/-}$ mice showed a significantly reduced outward remodeling response as compared with arteries from wild-type mice (top part of graph). In arteries chronically exposed to decreased flow (LF arteries), no differences in inward remodeling were noted (bottom part of graph). *, $P<0.05$ in two-way ANOVA. $n=5$ animals for *Gja5*$^{-/-}$ and wild type; from each animal, one HF, one LF and one NF vessel was isolated and investigated in the arteriograph.

Fig. S9. Expression of Gja5 in the hindlimb. (**A**) Changes in Gja5 expression after femoral artery occlusion. Gja5 expression is shown as the ratio of expression in the ischemic hindlimb and the control hindlimb, using the gastrocnemius muscle of wild-type and *Gja5*$^{+/-}$ mice ($n=3$ animals per group). At 3 days after occlusion, expression was elevated 4-fold in the ischemic hindlimb, both in *Gja5*$^{+/-}$ and wild type. Expression levels returned to baseline values at 7 days after occlusion. (**B**) PCR on DNA isolated from femoral artery after tamoxifen treatment to prove deletion of the *Gja5* gene in conditional *Gja5*$^{flox/flox}$ mutants crossed with inducible *Tie2 Cre* mice. Upper lane illustrates the presence of Cre in Cre^{+} but not Cre^{-} mice. *Gja5*-floxed band could be

detected in tail DNA before tamoxifen treatment in both the Cre^{+}*Gja5*-floxed mouse and the Cre^{-}*Gja5*-floxed littermate (middle lane). But after tamoxifen treatment, only the Cre^{+} mouse shows a *Gja5* deletion band (lower lane). FA, femoral artery. (**C**,**D**) Reduced expression of Gja5 after endothelial specific deletion of *Gja5*. Mice were treated once daily, during 2 weeks, with tamoxifen prior to performing FAO. Expression was measured in the femoral artery (C) and gastrocnemius muscle (D). *, $P<0.05$, $n=3$ animals per group, *t*-test. Tc+ gja5f/f, inducible Cre^{+}*Gja5*$^{flox/flox}$ mice treated with tamoxifen. Tc− gja5f/f, inducible Cre^{-}*Gja5*$^{flox/flox}$ mice treated with tamoxifen.

Table S1. Primer sequences for conditional *Gja5* mutant mouse genotyping and *Gja5*, *Dll4* quantitative real-time PCR analysis (in Fig. S5B)

	Forward primer	Reverse primer
Cre PCR	GCGGTCTGGCAGTAAAAACTATC (Cre-F)	GTGAAACAGCATTGCTGTCACTT (Cre-R)
Gja5 floxed	GGCCATCCTCTGCTACATATGCAG (Gja5-flox-F)	GTGACATGACCTGGATCTCTGGAG (Gja5-flox-R)
Gja5 deletion	GGCCATCCTCTGCTACATATGCAG (Gja5-flox-F)	AGTAGTGCTGAGGAGAGTA (Gja5-ko-R)
Dll4 chicken	CGCCATGGGACTTGTAAAAC	TTGCATGGTCTGTGGTGAGT
Gja5 chicken	AAAGAGAGGCCGTCTCCAAT	TGTGGACCTCCTCAAGGAAC

Fig. S1

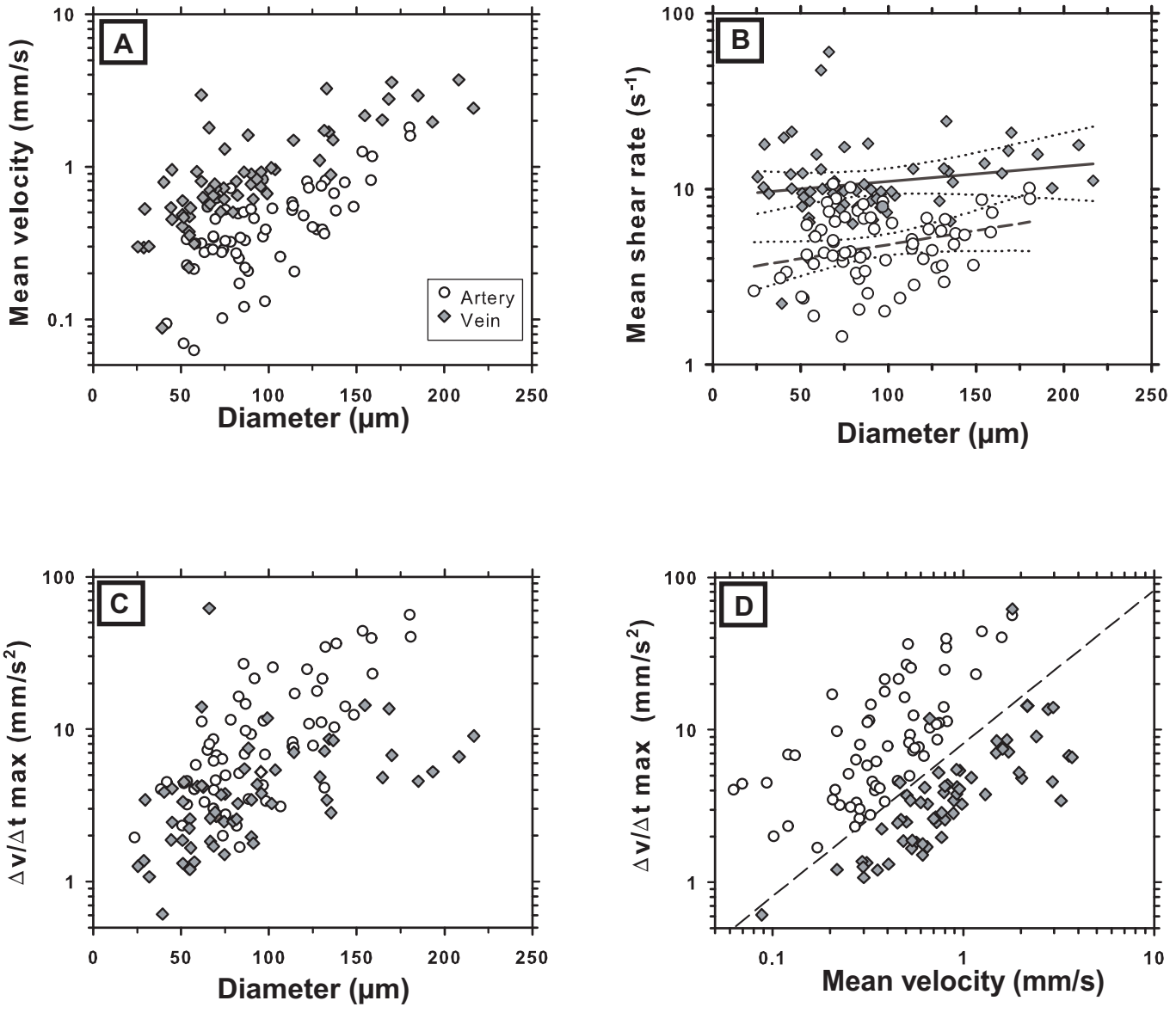
A
Mean velocity (mm/s)
10
1
0.1
0
50
100
150
200
250
Diameter (μm)
Artery
Vein
B
Mean shear rate (s-1)
100
10
1
Diameter (μm)
C
Δv/Δt max (mm/s2)
100
10
1
Diameter (μm)
D
Δv/Δt max (mm/s2)
100
10
1
0.1
1
10
Mean velocity (mm/s)

Fig. S2

Receiver Operator Characteristics (ROC) analysis

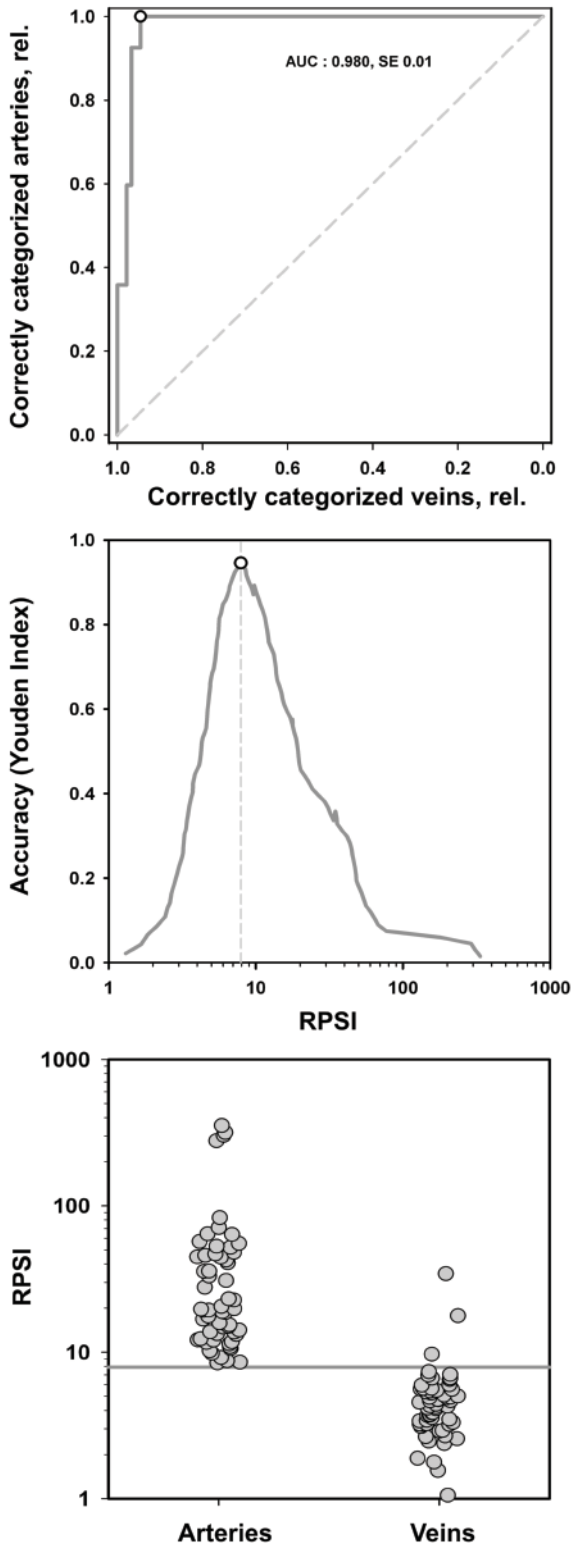

Fig. S3

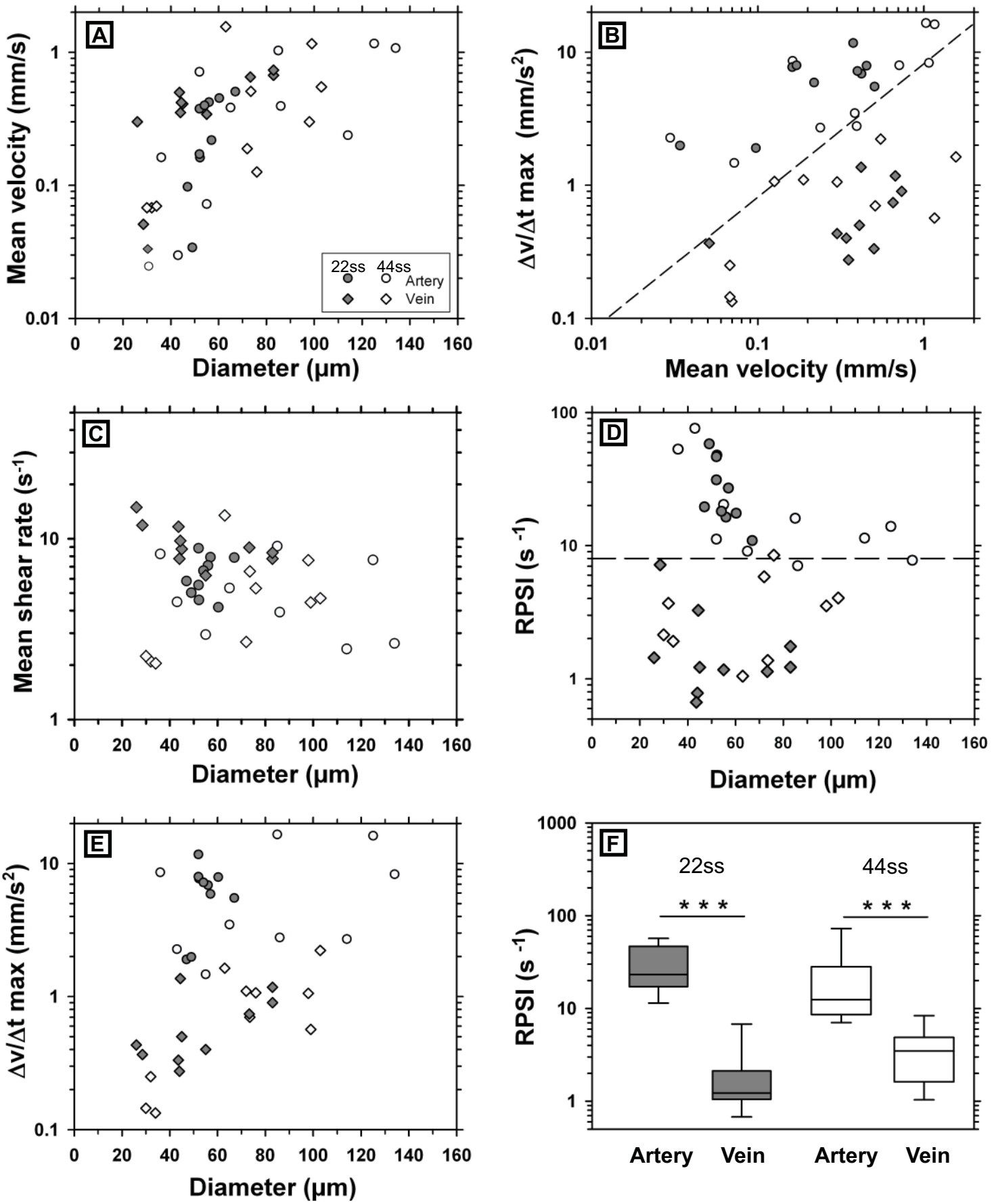
A
Mean velocity (mm/s)
Diameter (μm)
22ss 44ss
Artery
Vein
B
Δv/Δt max (mm/s²)
Mean velocity (mm/s)
C
Mean shear rate (s⁻¹)
Diameter (μm)
D
RPSI (s⁻¹)
Diameter (μm)
E
Δv/Δt max (mm/s²)
Diameter (μm)
F
RPSI (s⁻¹)
22ss
44ss
* * *
* * *
Artery
Vein
Artery
Vein

Fig. S4

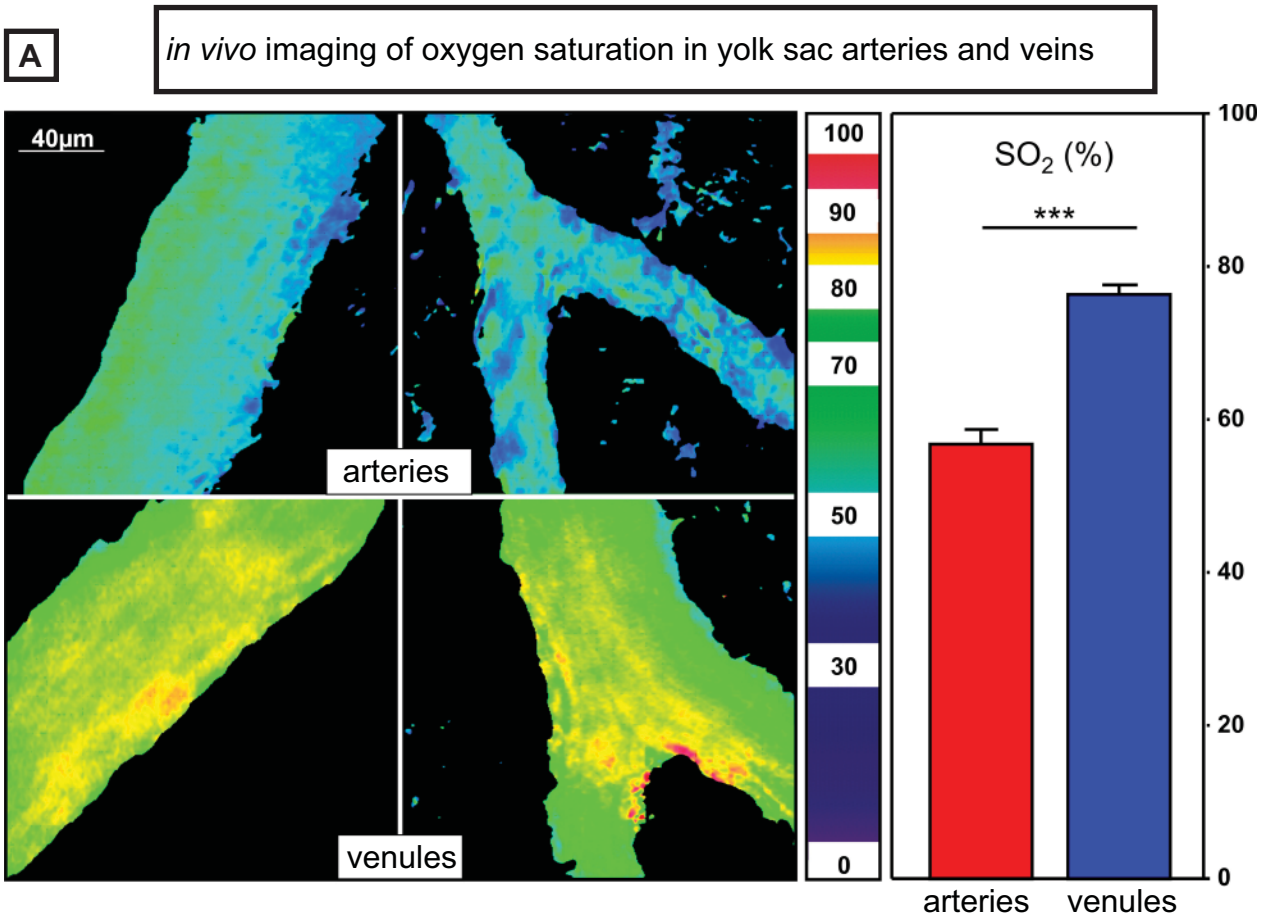
A
in vivo imaging of oxygen saturation in yolk sac arteries and veins
40µm
arteries
venules
100
90
80
70
50
30
0
SO2 (%)
***
100
80
60
40
20
0
arteries
venules
B
normoxia
hypoxia
LVA
RVA
vein
LVA
RVA

Fig. S5

A

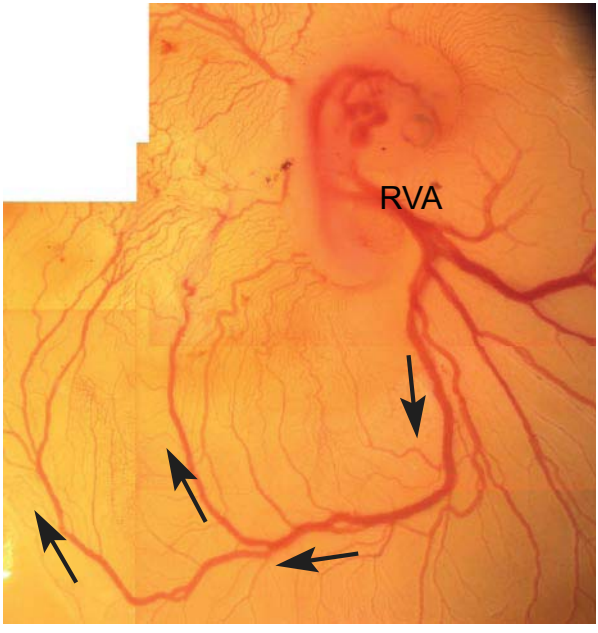

B

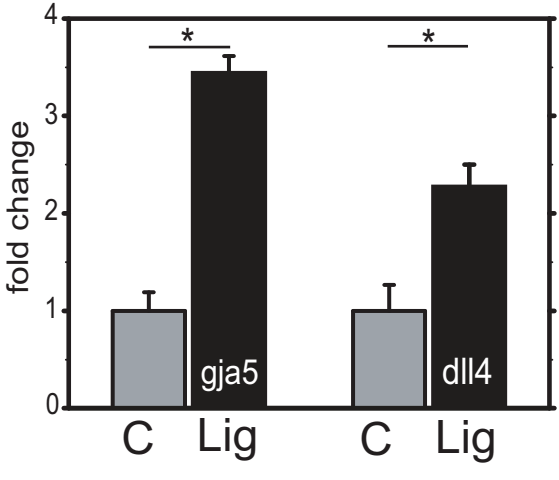

Fig. S6

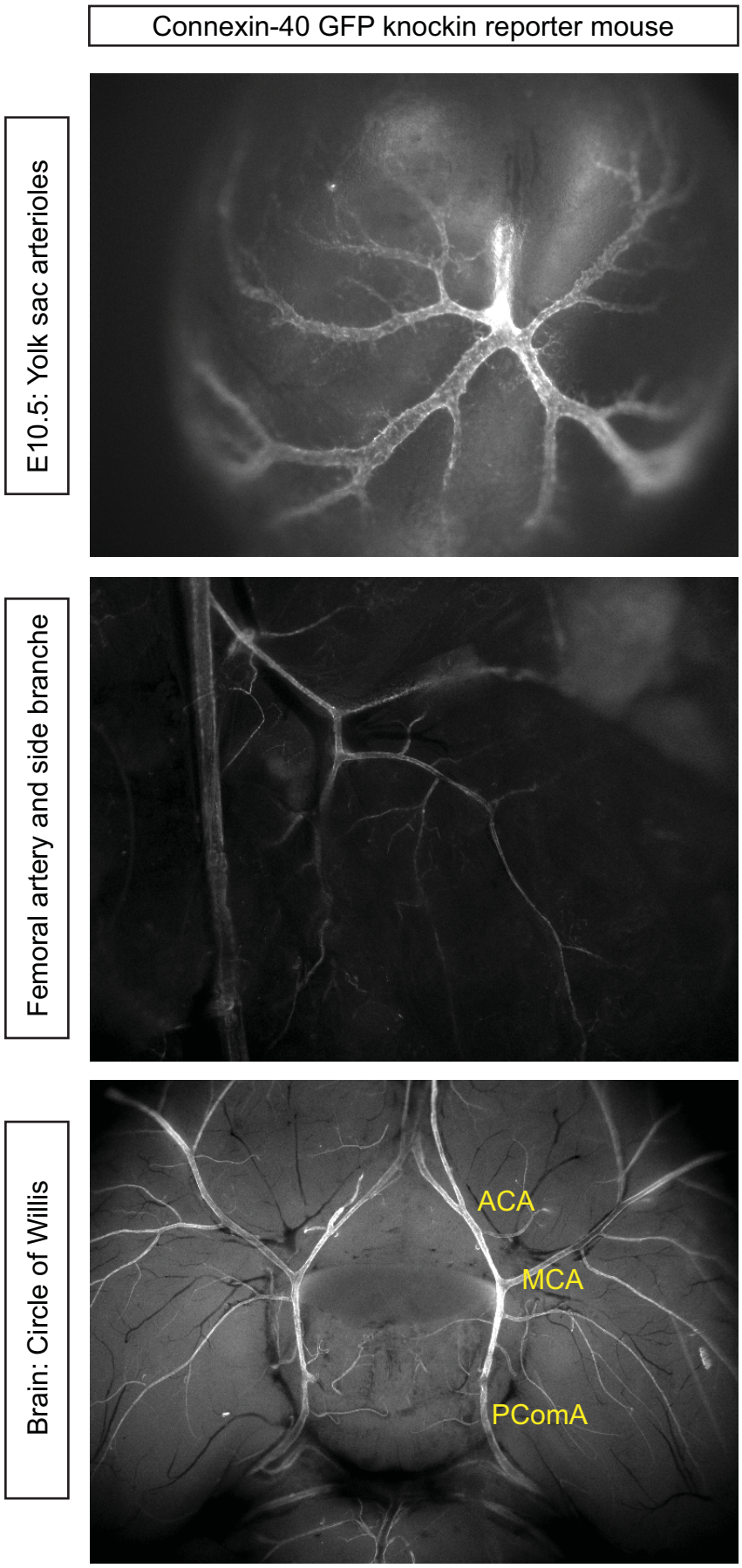
Connexin-40 GFP knockin reporter mouse
E10.5: Yolk sac arterioles
Femoral artery and side branche
Brain: Circle of Willis
ACA
MCA
PComA

Fig. S7

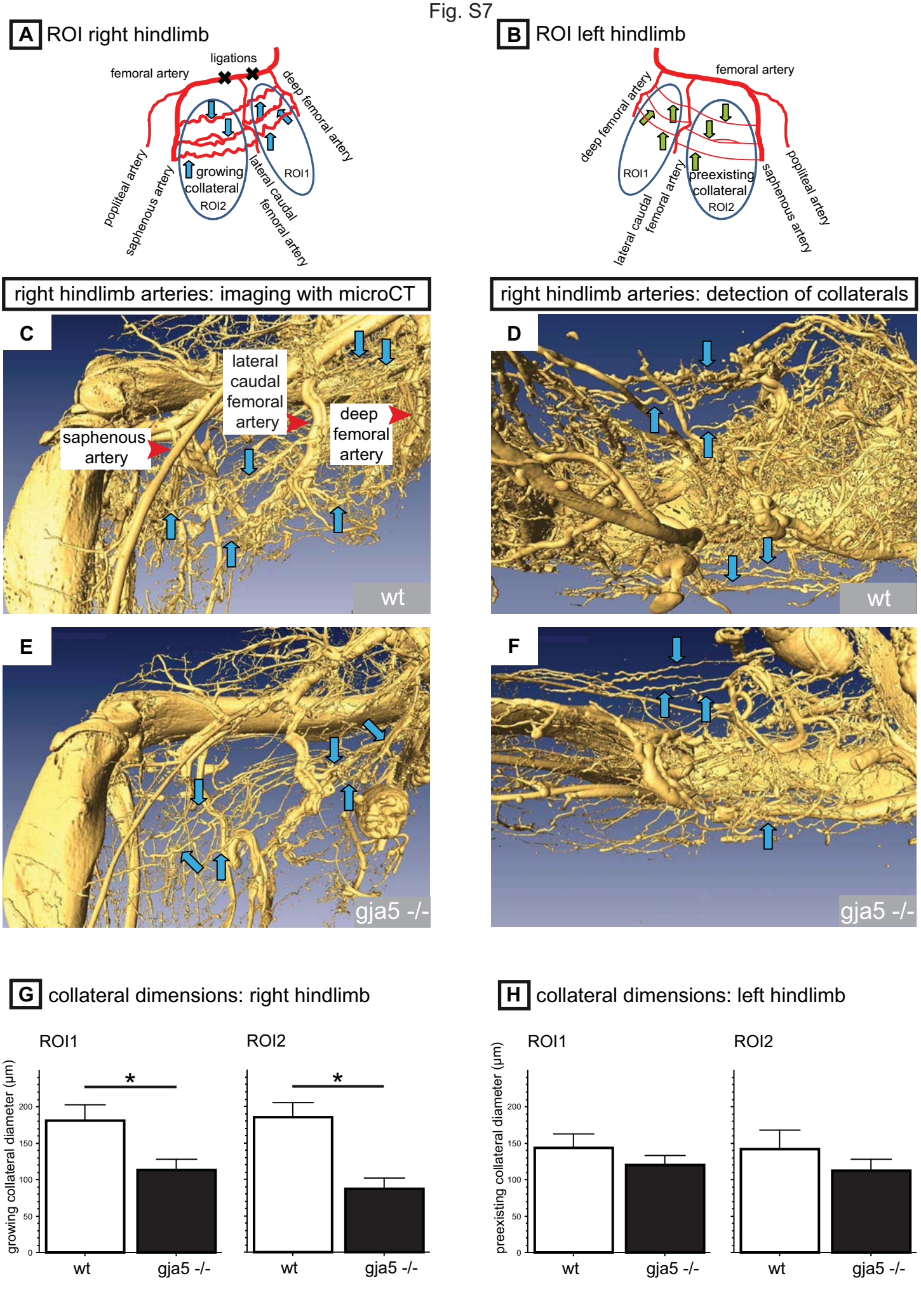
A ROI right hindlimb
ligations
femoral artery
deep femoral artery
popliteal artery
saphenous artery
growing collateral
ROI2
ROI1
lateral caudal femoral artery
B ROI left hindlimb
femoral artery
deep femoral artery
ROI1
preexisting collateral
ROI2
popliteal artery
saphenous artery
lateral caudal femoral artery
right hindlimb arteries: imaging with microCT
right hindlimb arteries: detection of collaterals
C
lateral caudal femoral artery
deep femoral artery
saphenous artery
wt
D
wt
E
gja5 -/-
F
gja5 -/-
G collateral dimensions: right hindlimb
ROI1
ROI2
growing collateral diameter (µm)
0
50
100
150
200
*
*
wt
gja5 -/-
wt
gja5 -/-
H collateral dimensions: left hindlimb
ROI1
ROI2
preexisting collateral diameter (µm)
0
50
100
150
200
wt
gja5 -/-
wt
gja5 -/-

Fig. S8

A

flow induced arterial remodeling in the mesenteric model

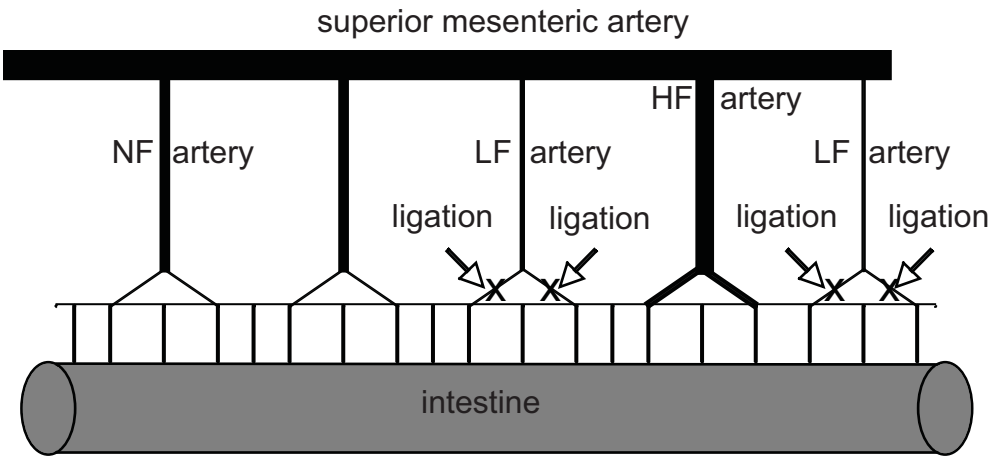

B

reduced outward remodeling in gja5-/- arteries

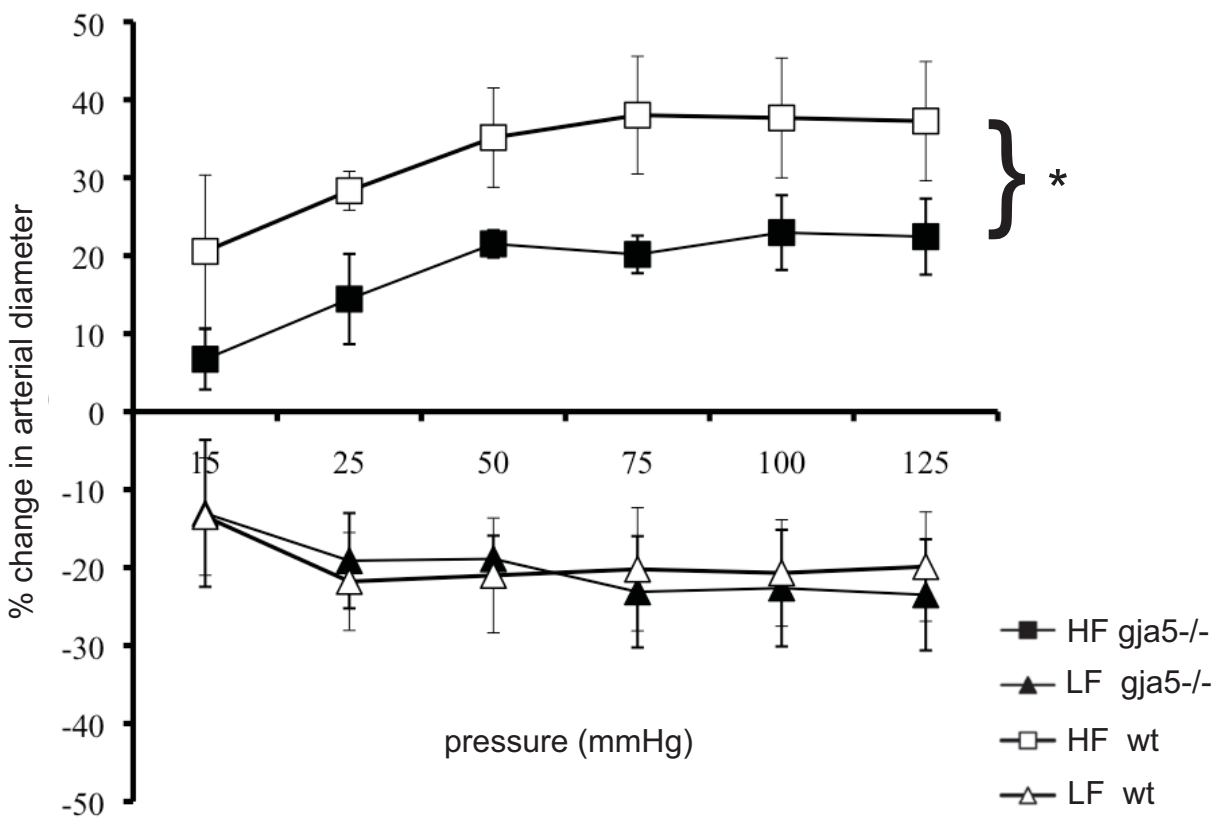

Fig. S9

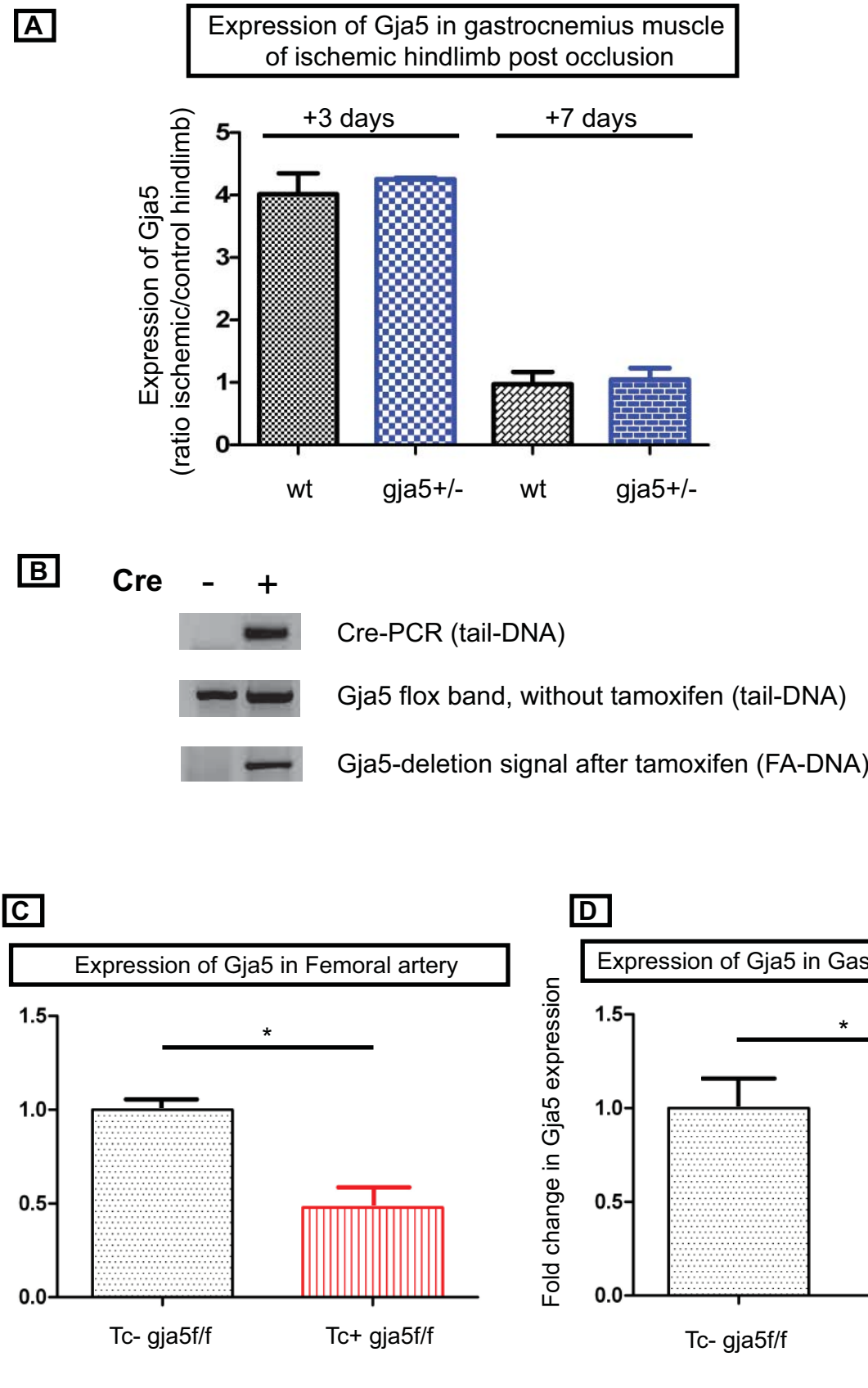
A
Expression of Gja5 in gastrocnemius muscle of ischemic hindlimb post occlusion
+3 days
+7 days
Expression of Gja5 (ratio ischemic/control hindlimb)
5
4
3
2
1
0
wt
gja5+/-
wt
gja5+/-
B
Cre - +
Cre-PCR (tail-DNA)
Gja5 flox band, without tamoxifen (tail-DNA)
Gja5-deletion signal after tamoxifen (FA-DNA)
C
Expression of Gja5 in Femoral artery
Fold change in Gja5 expression
1.5
1.0
0.5
0.0
*
Tc- gja5f/f
Tc+ gja5f/f
D
Expression of Gja5 in Gastrocnemius muscle
Fold change in Gja5 expression
1.5
1.0
0.5
0.0
*
Tc- gja5f/f
Tc+ gja5f/f